STEREO EVALUATION OF ALOS/PRISM DATA ON ESA-AO TEST SITES – FIRST DLR RESULTS

Mathias Schneider, Manfred Lehner, Rupert Müller, Peter Reinartz

German Aerospace Center (DLR), Remote Sensing Technology Institute, D-82234 Wessling, Germany
e-mail: {Mathias.Schneider, Manfred.Lehner, Rupert.Mueller, Peter.Reinartz}@dlr.de

Commission I, WG I/5

ABSTRACT:

DLR's Remote Sensing Technology Institute has more than 20 years of history in developing spaceborne stereo scanners (MEOSS, MOMS) and the corresponding stereo evaluation software systems. It takes part in the ESA/JAXA-AO Program to evaluate the performance and potential of the three-line stereo scanner PRISM (Panchromatic Remote-sensing Instrument for Stereo Mapping) and the multispectral imaging sensor AVNIR-2 onboard the Japanese satellite ALOS as a principal investigator. German (Southeast Bavaria) and Spanish (Catalonia) test sites are proposed for which also PI evaluations for the SPOT-5 HRS Scientific Assessment Program (SAP) had been done already in 2003/04, and for the Indian CARTOSAT-1 (C-SAP) from 2006 onwards. In this paper, the process of direct georeferencing according to JAXA is shown and first results are presented. Ground control points (GCPs) are used to estimate boresight angles to improve the accuracy of the direct georeferencing. Rational polynomial coefficients (RPCs) are generated using DLR software. The comparison of a GCP-based approach and the rigorous approach reveals an oscillation of the satellite in the order of up to one pixel on the ground. The oscillations can not be compensated by an RPC-based approach. DEMs are generated and the coregistration of forward, nadir and backward view is examined. Thereby, problems in the processing of the interior orientation are revealed.

1. INTRODUCTION

In the last years, the number of high resolution and very high resolution satellites increased and will further increase. For the orthorectification of the data gathered by these satellites, a DEM of sufficient accuracy is necessary. Up to now, the DEM produced by the Shuttle Radar Topography Mission (SRTM) is the best globally available DEM. However, with a resolution of 1-3 arc seconds, the potential of very high resolution imagery cannot be fully exploited. The PRISM instrument on the Japanese satellite ALOS combines high resolution imagery (2.5 m) with the capability to generate DEMs by providing three optical line scanners. Due to the experience of DLR's Remote Sensing Technology Institute (IMF) in developing spaceborne stereo scanners (MEOSS, MOMS) and the corresponding stereo evaluation software systems (Kornus et al, 2000), processing chains for three-line scanners already exist that can be adapted to PRISM data. In (Kocaman, Gruen, 2007), orientation parameters are estimated using ground control points (GCPs) and self-calibration is performed. (Kamiya, 2007) also performed a bundle adjustment on the PRISM data.

In this paper, the DLR approach to orthorectify PRISM imagery and calculate DEMs from PRISM images is shown and first results are presented. For the processing, the image processing software XDIBIAS, developed at IMF, is used as well as a newly developed tool for the interpretation of PRISM housekeeping data.

2. THE PRISM INSTRUMENT

The PRISM instrument is one of three instruments onboard of the Japanese satellite ALOS (nickname "Daichi") which was launched in January 2006. The other instruments are AVNIR-2, a multispectral radiometer, and PALSAR, a radar sensor. PRISM consists of three independent radiometers for nadir (N), backward (B) and forward (F) view. Each radiometer is composed of 6 (N) – 8 (F, B) CCD-arrays containing 4992 or 4928 pixels for nadir or forward/backward views respectively. There is a nominal overlap of 32 pixels between two neighboring CCD-arrays. Usually, an image is acquired using a subset of 4 consecutive CCD-arrays. The pixels, which are not used on the right and left CCD-array respectively, are regarded as so called dummy pixels and not used for the processing. A spatial resolution of 2.5 m is provided.

Wavelength	0.52-0.77 micrometers (Panchromatic)
Base to height ratio	1.0 (between F and B view)
Resolution	2.5 m
Swath width	35 km in triplet mode
Pointing angle	-1.5 to 1.5 degree
Stereo angle	+/- 23.8 degree (F/B)
Flying height	691650 m
Focal length	1.939 m
Number of CCDs	6 (N)/8 (F/B)
Pixel per CCD array	4992 (N)/4928 (F/B)

Table 1: Characteristics of ALOS/PRISM

View angles of +/- 23.8 degree for forward and backward view with respect to the nadir view result in a base-to-height ratio of one (Tadono et al, 2004). In table 1, the characteristics of ALOS/PRISM are given. Figure 2 shows the observation

geometry of the PRISM instrument. Since the aim was to generate DEMs, for this paper, only the triplet mode was examined.
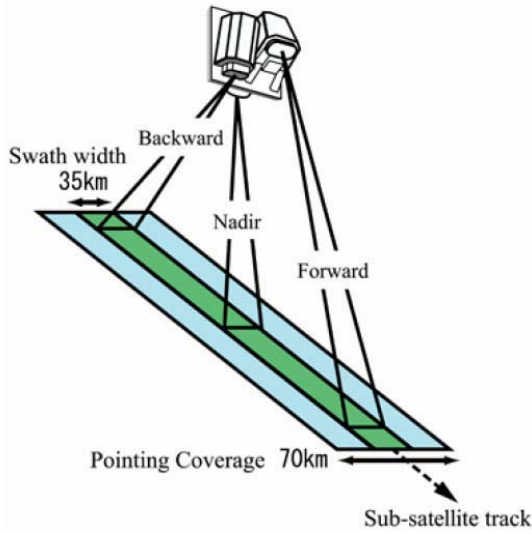

Figure 2: Observation geometry of triplet mode (Tadono et al., 2004).

3. DATA FORMAT

PRISM data can be delivered in different stages of processing: Level 1A, where no correction is done, Level 1B1, where the images are radiometrically corrected and Level 1B2, where the images are radiometrically and geometrically corrected. Imagery and ancillary data are given in CEOS format, partly in ASCII and partly in binary code.

For our purposes, Level 1B1 data are the most suitable ones. Level 1A and 1B1 images are composed by one image file per CCD with an overlap of 32 pixels. The image is thus created by merging the 4 image files together and the overlap is accounted for by cutting off 16 pixels of the overlap area of each image file. The column number of the composed image is then 14496. The image data itself is JPEG compressed on board of the satellite. Compression artifacts are visible in the imagery. To minimize the artifacts, a filter can be applied. E.g., an image enhancement software can be downloaded at (Kayima, 2006). We applied a 3x3 Gaussian filter before matching the images, which increases the quality of the matching results.
The imaging time for each line is given in the image files, while the ancillary data needed for our purposes is written in the SUP-file. According to (JAXA, 2006a), the following data are extracted: Precision orbit (ancillary 8), precision attitude (ancillary 12), coordinate conversion matrices (ancillary 10) and geometric parameter (ancillary 13).

4. TEST DATA

Different test datasets are used. One test site is located near Barcelona in Catalonia, Spain. Beside two sets (F, N, B) of PRISM L1B1 images, 5 orthophotos, provided by the Institut Cartogràfic de Catalunya (ICC), are available for GCP and ICP measurement as well as a DEM of the test site, also provided by ICC. The PRISM images were acquired in October 2006,

ordered via ESA and therefore also processed by the ESA processor. Unfortunately, the processor used at ESA was not updated when processing the data. Especially the parameters of the pointing alignment, which are used to calculate the interior orientation, have to be updated, before an efficient use of the data.

Therefore, a second test data set was provided by GAEL Consultant. The PRISM L1B1 images show the coastal region of Marseille in the south of France and were acquired in March 2007. The coordinates of six GCPs were provided, measured with GPS, as well as a DEM with 100 m resolution. This PRISM dataset was processed at JAXA with the JAXA processor.

5. DIRECT GEOREFERENCING

Unlike other papers (e.g. Kocaman, Gruen, 2007), we tried to follow the processing given in (JAXA, 2006b). Therefore, in the first step, the view vector u_{CCD} for each pixel in the CCD coordinate system is calculated as follows:

$$u_{CCD} = \frac{1}{\sqrt{1 + dx^2 + dy^2}} \begin{pmatrix} dx \\ dy \\ 1 \end{pmatrix} \tag{1}$$

where
$$dx = \tan(\theta_Y(k)) \tag{2}$$
$$dy = -\tan(\theta_X(k))$$

and

$$\theta_X(k) = \frac{k_2 - k}{k_2 - k_1}\theta_X(k_1) + \frac{k - k_1}{k_2 - k_1}\theta_X(k_2) + a_X\left(k - \frac{k_1 + k_2}{2}\right)^2 - b_X \tag{3}$$

$$\theta_Y(k) = \frac{k_2 - k}{k_2 - k_1}\theta_Y(k_1) + \frac{k - k_1}{k_2 - k_1}\theta_Y(k_2) + a_Y\left(k - \frac{k_1 + k_2}{2}\right)^2 - b_Y$$

k_1, k_2 are the pixel numbers at the measurement points, while k is the actual pixel number and is computed as follows:

$$k(i) = (CCD\_no - 1)(pix - 32) + left\_dummy\_pix + i \tag{4}$$

where
$\quad$ pix = 4992 in case of a nadir image and
$\quad$ pix = 4928 for forward/backward view and

$$\theta_X(k_i) = \theta_{X0i} + \delta\theta_{X0i} \qquad \text{for i} = \{1,2\} \tag{5}$$
$$\theta_Y(k_i) = \theta_{Y0i} + \delta\theta_{Y0i}$$

The values for $k_i, \theta_{X0i}, \theta_{Y0i}, \delta\theta_{X0i}, \delta\theta_{Y0i}$ are retrieved from the SUP-file, ancillary 13, as well as the values for a_X, b_X, a_Y, b_Y, which account for the CCD distortion.
This view vector is then transformed to the earth centered rotated coordinate system (ECR) ITRF97 u_{ECR}.

$$u_{ECR} = QMAu_{CCD} \tag{6}$$

where

$$Q = R_{XY} R_{GAST} R_{PN} \tag{7}$$

R_{XY} is built using the information for polar motion (XY-matrix part), R_{GAST} is built using the Greenwich Apparent Sidereal Time information and R_{PN} is built using the precession/nutation information (PN-matrix part). The needed information is given in the SUP-file, ancillary 10. Q is the matrix that transforms a vector from earth centered inertial coordinate system (ECI) J2000 to ECR.

Matrix M(q) is built using the quaternions from precision attitude, also given in the SUP-file (ancillary 12), as follows:

$$M(q) = \begin{pmatrix} 1-2(q_2^2 + q_3^2) & 2(q_1q_2 - q_0q_3) & 2(q_1q_3 + q_0q_2) \\ 2(q_1q_2 + q_0q_3) & 1-2(q_1^2 + q_3^2) & 2(q_2q_3 - q_0q_1) \\ 2(q_1q_3 - q_0q_2) & 2(q_2q_3 + q_0q_1) & 1-2(q_1^2 + q_2^2) \end{pmatrix} \tag{8}$$

Roll pitch and yaw angles are extracted from M(q) as follows:

$$roll = -\arcsin(M_{23}) \tag{9}$$

$$pitch = \arctan(\frac{M_{13}}{M_{33}})$$

$$yaw = \arctan(\frac{M_{21}}{M_{22}})$$

The angles at imaging time are computed by linear interpolation. The matrix M at imaging time is then built as follows:

$$M = R_y(pitch)R_x(roll)R_z(yaw) \tag{10}$$

where

$$R_x(roll) = \begin{pmatrix} 1 & 0 & 0 \\ 0 & \cos(roll) & -\sin(roll) \\ 0 & \sin(roll) & \cos(roll) \end{pmatrix}$$

$$R_y(pitch) = \begin{pmatrix} \cos(pitch) & 0 & \sin(pitch) \\ 0 & 1 & 0 \\ -\sin(pitch) & 0 & \cos(pitch) \end{pmatrix} \tag{11}$$

$$R_z(yaw) = \begin{pmatrix} \cos(yaw) & -\sin(yaw) & 0 \\ \sin(yaw) & \cos(yaw) & 0 \\ 0 & 0 & 1 \end{pmatrix}$$

M is the matrix that transforms a vector from satellite coordinate system to ECI. The matrix A is built from various information given in the SUP-file, ancillary 13.

$$A = (n_0 A_{STT})^{-1} (nAn_0)^{-1} \Delta R(I, n) \tag{12}$$
where

$$n_0 A_{STT} = \begin{pmatrix} 1 & \psi nl & -\theta nl \\ -\psi nl & 1 & \phi nl \\ \theta nl & -\phi nl & 1 \end{pmatrix} \begin{pmatrix} an11 & an12 & an13 \\ an21 & an22 & an23 \\ an31 & an32 & an33 \end{pmatrix} \tag{13}$$

where the coefficients an11-an33 account for the mount angles of the optics, stereo angles, etc.. The coefficients in the first matrix represent the long period bias time variation by a linear expression of the number of days since the start date. However, in the test datasets, they were zero.

$$nAn_0 = \begin{pmatrix} 1 & \psi n & -\theta n \\ -\psi n & 1 & \phi n \\ \theta n & -\phi n & 1 \end{pmatrix} \tag{14}$$

where the coefficients are computed by a polynomial of degree 30 of the dimensionless number s, which normalizes the time, when the satellite is in sunshine, by the orbit period of 98.7 minutes. The polynomial coefficients are also given in the SUP-file, ancillary 13.

$$\Delta R(I, n) = \begin{pmatrix} 1 & \Psi(I, n) & -\theta(I, n) \\ -\Psi(I, n) & 1 & \phi(I, n) \\ \theta(I, n) & -\phi(I, n) & 1 \end{pmatrix} \tag{15}$$

where the coefficients are given for each CCD (n) and each radiometer (I) in the SUP-file, ancillary 13. The matrix eliminates the differences between CCD coordinate system defined in the PRISM sensor model and the reference CCD coordinate system for the pointing alignment parameters. However, in the test datasets, the coefficients were zero.

5.1 Interior Orientation

To use the existing programs at DLR, some modifications had to be made. Exterior and interior orientations have to be given for each line and each pixel respectively. Therefore, equation (6) is split up in two parts. The interior orientation has to be given in a table as view vector for each pixel according to equation (16).

$$u_{int} = Au_{CCD} \tag{16}$$

To be compatible with the existing DLR software, the sign of the z-component of the view vector is changed.

5.2 Exterior Orientation

The exterior orientation consists of the angles for roll, pitch and yaw and of the satellite position at imaging time in ECR coordinates. This information has to be given for each imaging line. The angles are extracted from the first part of equation (6), the product of Q and M, as described in equation (9). Since in the existing DLR programs, the definition of the direction of the rotation is different, the signs of the extracted angles are changed.

The satellite position and velocity is given as precision orbit data in the SUP-file, ancillary 8, both in ECI and ECR coordinates for every minute. The position at imaging time is calculated using a Hermite interpolation, considering the 4 data points around the point of interest.

$$x(t) = \sum_{i=1}^{4}(x_i F_{0i} + \dot{x}_i F_{1i})H_i^2 \qquad (17)$$

where

$$H_i = \prod_{k \neq i} \frac{t - t_k}{t_i - t_k}$$

$$F_{0i} = 1 - 2(t - t_i)\sum_{j \neq i}\frac{1}{t_i - t_j} \qquad (18)$$

$$F_{1i} = t - t_i$$

where x is the orbit position vector and t the time of interest.

5.3 Tests

To check the correctness of our processing, the coordinates of the upper left pixel are calculated without the modifications that were made to adapt the data to DLR software. This coordinate is then compared to the coordinate calculated using the coefficients given in the LED-file, ancillary 1. These coefficients were e.g. used for Cal/Val tests (Saunier, 2007).
For the Catalonian test site, the difference is approximately 240 m, mainly in flight direction. For the French test site, the difference is smaller, but still in the order of approximately 60 m, also mainly in flight direction. This difference results probably from the different versions of processors used. Especially the pointing alignment parameters given in the SUP-file, ancillary 13 have changed.

We thus decided to use GCPs to estimate boresight angles using the DLR developed software ESTIMATE.

5.4 RPC Generation

Since for a RPC-based approach no new software had to be developed, the first idea was to generate RPCs for the PRISM images. Therefore, a three dimensional grid of control points is generated over the whole image from the exterior and interior orientation. This is done by a modification of the software ORTHO, developed at DLR (Müller, 2005). The estimated boresight angles are used as input for ORTHO.

The RPCs are then computed as described in (Lehner, 2007), using XDIBIAS RPC generation software, developed at DLR. To check the RPCs, coordinates of the control points were recalculated using the RPCs and compared to the original coordinates. Figure 3 shows the plot of these residual vectors for a nadir image of a test site in Catalonia/Spain.

The results are similar for forward and backward images as well as for other test sites (Germany, France). The residuals are smaller than one pixel; however, they may affect the DEM-generation. Regarding the residual behavior in row direction, there seems to be an oscillation with an amplitude of approximately one pixel. In order to find the reason for this oscillation, the attitude angles are examined.
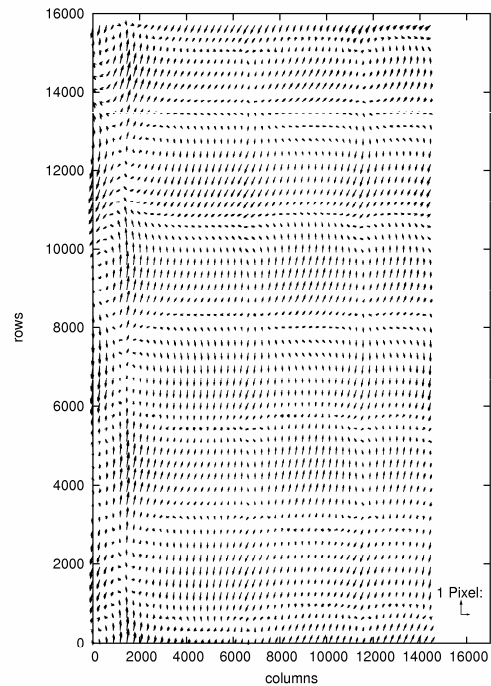

Figure 3: Residuals between original control point coordinates and those calculated by RPCs for nadir image of Catalonian test site.
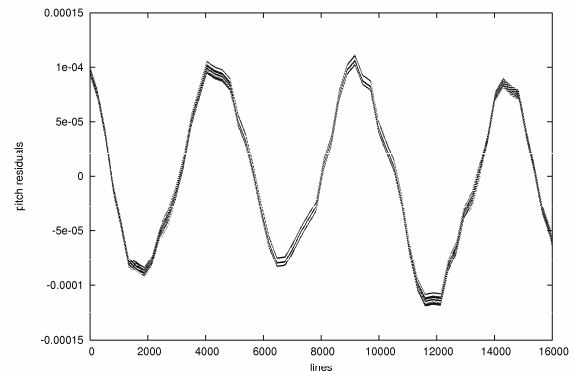

Figure 4: Residuals of pitch angle after subtracting a second degree polynomial for nadir image of Catalonian test site. Values are in degree.

When plotting the attitude angles for an image, they seem to have a linear behavior. However, when we estimate a second degree Legendre polynomial as trend line and subtract it from the original values, an oscillation is clearly visible. Figure 4 shows the residuals in pitch angle for the nadir view of the test site in Catalonia/Spain. The amplitude of the oscillation is small, however, in the images, it results in deviations of up to one pixel. For the yaw angle, the plot looks similarly, while for the roll angles, the residuals are slightly smaller. The oscillation may result from vibrations caused by the satellites momentum wheels. A similar oscillation is also known from other cases, e.g. MOMS-2P (Lehner, 2003). Due to the high resolution of

PRISM, the effects of the oscillation are not negligible as they are for SPOT. The oscillation of up to one pixel might be tolerable for orthoimage generation; however it will surely affect the DEM generation from PRISM triplets. This makes the RPC-based approach not suitable for PRISM imagery, since the effects can not be handled by RPCs. The rigorous model should be used.

6.   STEREO PROCESSING

Due to a lack of time, a forward intersection using the rigorous model was not yet done with our test images. For the moment, the RPC approach was chosen, knowing that the oscillation described in 5.4 will occur. However, there are still other errors that obstruct our processing.

6.1   Forward, Nadir and Backward Co-Registration

For a French test site, orthoimages are produced using DLR developed orthoprocessing software ORTHO. A DEM is used for the orthorectification as well as 6 ground control points derived from GPS measurements that were available for this test area.
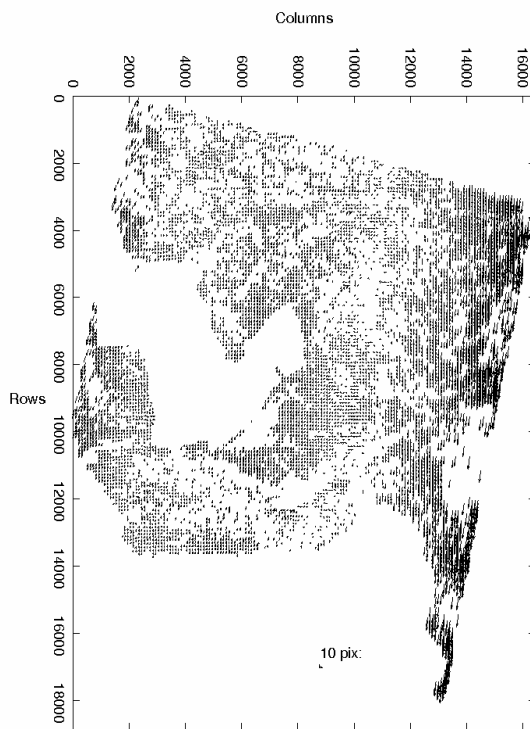

Figure 5: Residuals after matching of orthorectified nadir and backward view of French test site. 6 GCPs were used for the orthorectification.

The GCPs were used to estimate boresight angles that were introduced into the orthorectification process. A matching – originally developed for MOMS and MEOSS imagery (Kornus et al, 2000; Lehner, Gill, 1992) and further enhanced since then – between nadir and backward orthoimages was performed to display the quality of the coregistration of nadir and backward view. However, forward, nadir and backward view don't fit

exactly together. Figure 5 shows the residuals of the matching points of nadir and backward orthoimage.

The direction and dimension of the residuals varies over the image with up to 40 pixels in the eastern part of the images. Since possible errors in the exterior orientation angles should be eliminated by estimating the boresight angles, the remaining residuals might result from a distortion or shear of the images. The reason therefore can most probably be found in the interior orientation.

6.2   DEM Generation

For the Catalonian test site, chips of the images are used to calculate small DEMs using the RPC-based approach. Therefore, after a matching of forward, nadir and backward image, a forward intersection is computed for the tie points. Only three ray points are used. A DEM is then interpolated from the resulting mass points for each chip. The DEMs are then compared to the reference DEM provided by ICC. Figures 6 and 7 show this comparison across and in flight direction, respectively. The profiles show a good lateral correlation. However, regarding the height, they differ. For the profiles in flight direction, there is a constant offset between both profiles. In figure 7, this offset is about 50 m, in profiles at other positions in the image chip, it is very small.

For the profiles across the flight direction, there is no constant offset. As shown in figure 6, the difference between PRISM DEM and reference DEM ranges between 60 m and 0 m.
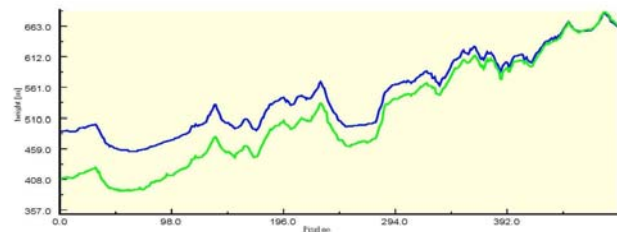

Figure 6: Comparison of a profile in PRISM DEM (green) and reference DEM (blue) for one chip in the north-western part of the images. The profile is across-track.
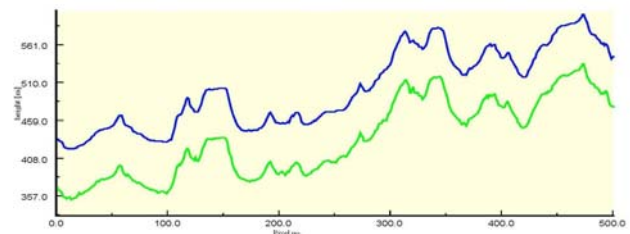

Figure 7: Comparison of a profile in PRISM DEM (green) and reference DEM (blue) for one chip in the north-western part of the images. The profile is along-track.

For the other image chips, the profiles look similarly. Since the offsets in flight direction are constant and the lateral correlation is high, the exterior orientation seems to be correct. However, there seem to be problems in the interior orientation, since

across flight direction, the difference in the profiles vary. The results from the nadir/backward coregistration tests also point on an error in the interior orientation. Probably there is a distortion or a misalignment between the CCD-arrays that is not modeled correctly by the pointing alignment parameters given in the SUP-file, ancillary 13.

Up to now, we could not identify the reason or find a correction of this effect. Further investigations on this problem will be done.

7. CONCLUSION

After extraction of ancillary data from ALOS PRISM files, orthoimages and DEMs can be created. In this paper, the way of direct georeferencing is shown, according to (JAXA, 2006b). Although the results improved when using the data processed with the more current JAXA processor instead of the ESA processor, tests showed that ground control points have to be used to estimate boresight angles.

It is shown, that an RPC-based approach reveals oscillation of up to one pixel in the image. While this might be tolerable for orthoimage generation for most applications, it will affect the DEM generation. The oscillation might probably result from vibrations caused by the satellites momentum wheels. Thus, we recommend the use of a rigorous approach rather than an RPC-based approach.

Additionally, there seem to be still problems in the interior orientation. Comparison of PRISM DEM and reference DEM show a constant offset in flight direction, while across flight direction, the differences vary in a huge range. This effect can also be detected when regarding the coregistration of nadir and backward view: The residual size and direction vary across flight direction, whereas they remain nearly constant in flight direction.
This effect will be investigated further in the future.

REFERENCES

JAXA, 2006a: ALOS PRISM Level 1 Product Format Descriptions Rev.J, October 2006. http://www.eorc.jaxa.jp/ALOS/doc/format.htm

JAXA, 2006b: ALOS Algorithm description (PRISM/AVNIR-2) Kamiya I., 2006: Study on ALOS PRISM, homepage: http://gisstar.gsi.go.jp/ALOS/index_e.html

Kamiya I., 2007: Geometric Characteristics of the Early Products of ALOS PRISM. Bulletin of the Geographical Survey Institute, vol.54, pp.75–82.

Kocaman S., Gruen A., 2007: Rigorous Sensor Modeling of ALOS/PRISM Imagery. 8th Conference on Optical 3D Measurement Techniques, Zurich, Switzerland, 9-12 July.

Kornus W., Lehner M. and Schroeder, M., 2000, Geometric inflight calibration by block adjustment using MOMS-2P 3-line-imagery of three intersecting stereo-strips, SFPT (Société Francaise de Photogrammétrie et Télédétection), Bulletin Nr. 159, pp. 42-54

Lehner M., Müller R., 2003. Quality Check of MOMS-2P Orthoimages of Semi-Arid Landscapes, Proceedings of ISPRS Worjshop on "High Resolution Mapping from Space 2003", October 6-8, Hannover, Germany

Lehner M. and Gill R.S., 1992. Semi-automatic derivation of digital elevation models from stereoscopic 3-line scanner data, IAPRS, Vol. 29, Part B4, Washington, USA, pp. 68-75.

Lehner M., Müller Ru., Reinartz P., 2005: DSM and Orthoimages from QuickBird and Ikonos Data Using Rational Polynomial Functions, Proceedings of "High Resolution Earth Imaging for Geospatial Information", May 17-20, Hannover, Germany

Lehner M., Müller R., Reinartz P., Schroeder M., 2007: Stereo evaluation of Cartosat-1 data for French and Catalonian test sites, Proceedings of the ISPRS Hannover Workshop 2007 High Resolution Earth Imaging for Geospatial Information, Hannover, Germany, May 29 – June 1

Müller, Ru.; Lehner, M.; Reinartz, P.; Schroeder, M.; 2005: "Evaluation of Spaceborne and Airborne Line Scanner Images using a generic Ortho Image Processor", Proc. of High Resolution Earth Imaging for Geospatial Information, ISPRS Hannover Workshop, Commision I WG 5, 2005 http://www.ipi.uni-hannover.de/fileadmin/institut/pdf/046-mueller.pdf

Saunier S., Demange C., Goryl, P., 2007: Final calibration/validation report PRISM. http://earth.esa.int/pub/ESA_DOC/ALOS011.pdf

Tadono T., Shimada M., Watanabe M., Hashimoto T., Iwata T., 2004: Calibration and Validation of PRISM Onboard ALOS. International Archives of Photogrammetry, Remote Sensing and Spatial Information Sciences, Vol.XXXV part B1, pp. 13-18.